BIOCHEMISTRY
including biophysical chemistry & molecular biology

Article

pubs.acs.org/biochemistry

# Structural Insight into the Mechanism of DNA-Binding Attenuation of the Neisserial Adhesin Repressor NadR by the Small Natural Ligand 4-Hydroxyphenylacetic Acid

Sébastien Brier, Luca Fagnocchi, Danilo Donnarumma, Maria Scarselli, Rino Rappuoli, Mikkel Nissum, Isabel Delany, and Nathalie Norais*

Research Center, Novartis Vaccines and Diagnostics, via Fiorentina 1, 53100, Siena, Italy

Supporting Information

**ABSTRACT:** Neisserial adhesin A (NadA) is a surface exposed trimeric protein present in most hypervirulent meningococcal strains and involved in epithelial cell adhesion and colonization. The expression of *nadA* is controlled by Neisserial adhesin regulator (NadR), a member of the MarR family, which binds to the *nadA* promoter and strongly represses the transcription of *nadA*. It was recently demonstrated that the DNA-binding activity of NadR was attenuated by 4-hydroxyphenylacetic acid (4-HPA), a natural molecule released in human saliva, thus leading to the de-repression of *nadA in vivo*. To elucidate the mechanism of regulation of NadR by 4-HPA, we used hydrogen−deuterium exchange mass spectrometry in association with *in silico* docking and site-directed mutagenesis. We show here that 4-HPA binds at the interface between the dimerization and the DNA-binding domains and stabilizes the homodimeric state of NadR without inducing large conformational changes in the DNA-binding lobes. The residues predicted to be in contact with 4-HPA were further selected for mutagenesis to assess their *in vitro* and *in vivo* functions in 4-HPA binding. Our results indicate that $Arg^{40}$ is critical for DNA-binding and reveal that $Tyr^{115}$ plays a key role in the mechanism of regulation of NadR by 4-HPA. Altogether our data suggest that the mechanism of regulation of NadR by 4-HPA mainly involves the stabilization of the dimer in a configuration incompatible with DNA binding.

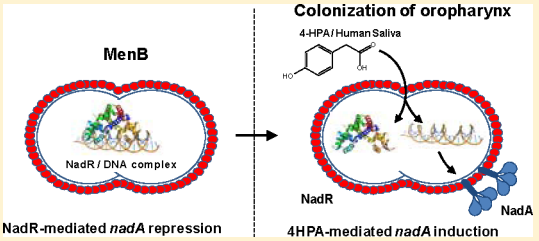


*Neisseria meningitidis* (Nm) is a strictly human pathogen which colonizes the oropharynx of about 10% of the population and causes in rare occasions an invasive infection leading to severe septicemia or meningitis.[1,2] In order to ensure colonization and dissemination, as well as to survive inside the host, Nm must be able to rapidly respond and adapt to changing environmental conditions by regulating the expression of genes involved in pathogenesis.[3,4] Although extensive transcriptional regulation is expected to occur in the infection process of Nm, only a few transcriptional regulators have been characterized to date and fewer still with respect to the molecular signals to which they respond *in vivo*.

Two of the 36 putative transcriptional regulators identified in Nm strain MC58 (according to the Comprehensive Microbial Resource database) belong to the multiple antibiotic resistance regulator (MarR) superfamily, NMB1585 and NMB1843. Members of this family regulate the activity of genes involved in a variety of cellular process including stress responses, metabolic pathways, antibiotic resistance, and virulence.[5−7] The main function of NMB1843 has been characterized.[8,9] NMB1843 (referred to as the Neisserial adhesin regulator, NadR) is responsible for repression of *nadA*, an important gene involved in Nm pathogenesis, whose gene product is the Neisserial adhesin A (NadA). NadA is implicated in colonization and invasion of the oropharynx and is included in the multicomponent 4CMenB vaccine developed to prevent disease caused by meningococcal serogroup B.[10−13] Recently, the NadR regulon has been elucidated and it has been demonstrated that NadR has a more global regulatory role during Nm infection.[14,15] In contrast to NadR, the physiological role of NMB1585 remains unknown (i.e., target genes and signal sensed) but its crystal structure has been recently solved.[16]

Members of the MarR family share the same core fold[6,7] and bind to the promoter region of their target genes as dimers leading to either transcriptional repression and/or activation.[7] A characteristic feature of the MarR family is their capability to bind and respond to a variety of effector molecules.[6,7] The interaction of ligands usually attenuates their DNA-binding activity, resulting in derepression of transcription,[7] but the opposite effect has also been reported.[17] Although the crystal structures of several MarR homologues have been solved in their apo- and ligand-bound states, we are still far from understanding the exact molecular mechanisms of regulation associated with ligand binding. This is partly because the natural ligand is often not known.

The majority of cocrystal structures of MarR homologues with ligands available in the Protein Data Bank (PDB) have been obtained with the molecule salicylate which, although a

**Received:** May 21, 2012
**Revised:** July 25, 2012
**Published:** July 26, 2012

 © 2012 American Chemical Society  dx.doi.org/10.1021/bi300656w | *Biochemistry* 2012, 51, 6738−6752

direct physiological relevance may not be apparent, binds to numerous MarR homologues albeit at very high concentrations.[18−22] Salicylate has been used as a general wildcard ligand to gain access to the mechanism of DNA-binding attenuation, but the biological relevance of much of the information gathered so far with this ligand has been questioned.[6] In contrast to many MarR homologues, NadR does not respond to salicylate.[8] It has been previously reported that the 4-hydroxyphenylacetic acid (4-HPA) molecule (Figure 1A), a catabolite of aromatic amino acids present in human saliva,[23,24] attenuates the *in vitro* DNA-binding activity of NadR and leads to *nadA* de-repression *in vivo*.[8] This natural compound is present in the host niche of Nm and is very likely to act as a natural ligand of NadR. Recently, this suggestion has been reinforced by the fact that human saliva itself induces *nadA* expression *in vivo*.[14] Given the importance of NadA in Nm pathogenesis, the 4-HPA molecule offers the unique opportunity to understand how a physiologically relevant signal present in human saliva may control its expression.

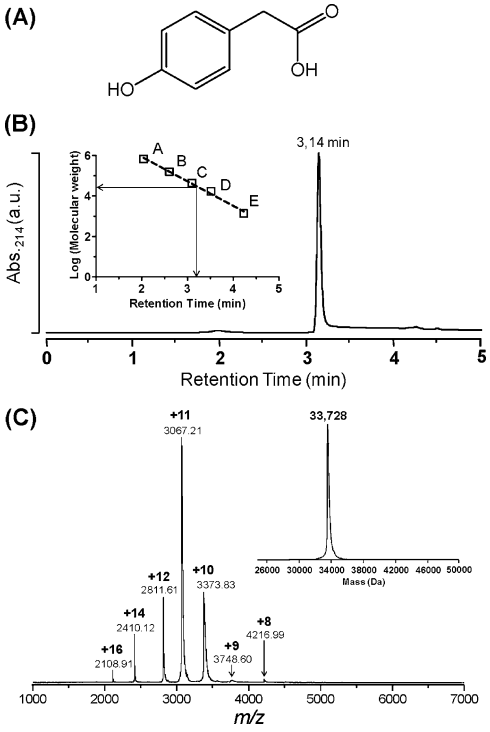


**Figure 1.** Structure of the 4-HPA ligand - oligomerization state of NadR. (A) Chemical structure of the 4-hydroxphenylacetic acid ligand (4-HPA) used in this study. (B) Size exclusion chromatogram of 10 $\mu$M purified NadR loaded onto a ACQUITY BEH200 SEC column (Waters) equilibrated with 50 mM sodium phosphate, pH 6.8, 300 mM NaCl. NadR is eluted as a single and symmetric peak with a retention time of 3.14 min corresponding to an estimated molecular weight of 35850 Da. The calibration curve obtained with a mixture of tyroglobulin (A, 670 kDa), $\gamma$-globulin (B, 158 kDa), ovalbumin (C, 44 kDa), myoglobin (D, 17 kDa), and vitamin B12 (E, 1350 Da) is also reported. (C) NanoESI mass spectrum of NadR (10 $\mu$M) under native conditions. The unique charge state distribution observed in the mass spectrum corresponds to the +8 to +16 charge states of NadR with a homodimeric organization. The measured molecular weight (33727.79 ± 0.4 Da) correlates with the expected mass of the homodimer (33728.16 Da).

In order to understand how 4-HPA regulates the DNA-binding activity of NadR, we used amide hydrogen/deuterium exchange mass spectrometry (HDX-MS) in association with *in silico* docking and mutagenesis. We show here that 4-HPA binds at the interface between the dimerization and the DNA-binding domains and stabilizes the homodimeric state of NadR without inducing large conformational changes in the DNA-binding lobes. The substitution of $Tyr^{115}$ located in the ligand-binding site prevents the 4-HPA-mediated stabilization of the dimer and suggests that occupancy of the HPA-binding pocket might be communicated to the dimerization interface and the DNA-binding lobes. The mechanism of regulation of NadR by 4-HPA deduced from our data is discussed and compared with the current available models of ligand-mediated regulation of MarR homologues.

## MATERIALS AND METHODS

**Materials.** Deuterium oxide (99.9 atom % D), sodium deuteroxide, deuterium chloride, 4-hydroxyphenylacetic acid, acetonitrile, Glu-fibrinogen peptide (GFP), and pepsin from hog stomach were all purchased from Sigma Aldrich and used without further purification. Standard coated Picotip emitters with a 1 $\mu$m tip inner diameter were obtained from New Objective.

**Bacterial Strains and Growth Conditions.** The Nm strains used in this study (Table 1) are all derivatives of the MC58 wild-type strain. They were routinely grown on GC (Difco) agar medium supplemented with Kellogg's supplement I at 37 °C/5% $CO_2$ overnight. When required erythromycin antibiotic was added to a final concentration of 5 $\mu$g/mL. For liquid cultures, Nm strains were grown overnight on solid medium, and a few colonies were inoculated in 7 mL of GC broth supplemented with Kellogg's supplement I to an initial optical density at 600 nm ($OD_{600}$) of 0.05.

**Generation of MC58 *nadR* Mutant Strains.** DNA manipulations were carried out routinely as described by Sambrook et al.[25] The previously described *nadR* null mutant MC58-Δ1843 strain[8] was complemented by the reinsertion of the *nadR* gene (NMB1843) under the control of the P*tac* promoter between the converging open reading frames NMB1428 and NMB1429, through transformation with the plasmid pComEry-1843 (Table 1). pCompEry-1843 is a derivative plasmid of pSLComCmr,[26] in which the *nadR* gene was amplified from the MC58 genome with the primer pair 1843-F and 1843-R2 (Table 2) and cloned as a 441-bp NdeI/NsiI fragment downstream of the P*tac* promoter. The chloramphenicol resistance cassette of pSLComCmr was substituted with an erythromycin resistance cassette, amplified with primers EryXbaF and EryBamR and cloned into the XbaI-*Bam*HI sites. The resulting MC58-Δ1843_C complemented mutant strain (Table 1) was selected on erythromycin. In order to generate MC58 mutant strains expressing only amino acid substituted forms of NadR, plasmids containing the sequence of *nadR* alternatively mutated in the codons coding for $Arg^{18}$, $Trp^{39}$, $Arg^{40}$, or $Tyr^{115}$ were constructed using the QuikChange II XL Site-Directed Mutagenesis kit (Stratagene). Briefly, the *nadR* gene was mutated in the pComEry-1843 plasmid using four couples of mutagenic primers (R18A-F/R18A-R, W39A-F/W39A-R, R40A-F/R40A-R, and Y115A-F/Y115A-R (Table 2)). The resulting plasmids were named pComEry-1843R18A, -1843W39A, -1843R40A, and -1843Y115A, and contain a site-directed mutant allele of the *nadR* gene, in which the $Arg^{18}$, $Trp^{39}$, $Arg^{40}$, and $Tyr^{115}$ codons were respectively substituted by


dx.doi.org/10.1021/bi300656w | *Biochemistry* 2012, 51, 6738−6752

**Table 1. Strains and Plasmids Used in This Study**

| strains | relevant characteristics | ref |
|---|---|---|
| *Neisseria meningitidis* | | |
| MC58 | clinical isolate, sequenced strain | 46 |
| MC58-Δ1843 | NadR null mutant in MC58 strain, CmR | 8 |
| MC58-Δ1843_C | MC58-Δ1843 derivative, NadR complemented strain expressing the *nadR* wild type gene under the control of the inducible P*tac* promoter between the converging open reading frames NMB1428 and NMB1429, EryR | this study |
| MC58-Δ1843_CR18A | MC58-Δ1843 derivative, NadR complemented strain expressing the *nadR* R18A mutant gene, EryR | this study |
| MC58-Δ1843_CW39A | MC58-Δ1843 derivative, NadR complemented strain expressing the *nadR* W39A mutant gene, EryR | this study |
| MC58-Δ1843_CR40A | MC58-Δ1843 derivative, NadR complemented strain expressing the *nadR* R40A mutant gene, EryR | this study |
| MC58-Δ1843_CY115A | MC58-Δ1843 derivative, NadR complemented strain expressing the *nadR* Y115A mutant gene, EryR | this study |
| *E. coli* | | |
| DH5-α | supE44 hsdR17 recA1 endA1 gyrA96 thi-1 relA1 | 47 |
| BL21(DE3) | hsdS gal (λcIts857 ind1 Sam7 nin-5 lacUV5-T7 gene 1) | 48 |
| Plasmids | | |
| pET15b | expression vector for N-terminal His tagged proteins, AmpR | Invitrogen |
| pET15-1843 | pET15b derivative for expression of recombinant 1843 protein, AmpR | 8 |
| pET15-1843R18A | pET15−1843 derivative for expression of recombinant 1843-R18A mutant protein, AmpR | this study |
| pET15-1843W39A | pET15-1843 derivative for expression of recombinant 1843-W39A mutant protein, AmpR | this study |
| pET15-1843R40A | pET15-1843 derivative for expression of recombinant 1843-R40A mutant protein, AmpR | this study |
| pET15-1843Y115A | pET15-1843 derivative for expression of recombinant 1843-Y115A mutant protein, AmpR | this study |
| pSLComCmr | plasmid consisting of the chloramphenicol resistance gene flanked by upstream and downstream regions for allelic replacement at a chromosomal location between ORFs NMB1428 and NMB1429, CmR | 26 |
| pComEry-1843 | plasmid for complementation of the NadR null mutant, derivative of pSLComCmr containing a copy of the nadr gene under the control of the $P_{tac}$ promoter, EryR | this study |
| pComEry-1843 R18A | plasmid for complementation of the NadR null mutant with the R18A mutant form of *nadR*, derivative of pComEry-1843, EryR | this study |
| pComEry-1843 W39A | plasmid for complementation of the NadR null mutant with the W39A mutant form of *nadR*, derivative of pComEry-1843, EryR | this study |
| pComEry-1843 R40A | plasmid for complementation of the NadR null mutant with the R40A mutant form of *nadR*, derivative of pComEry-1843, EryR | this study |
| pComEry-1843Y115A | plasmid for complementation of the NadR null mutant with the Y115A mutant form of *nadR*, derivative of pComEry-1843, EryR | this study |

**Table 2. Oligonucleotides Used in This Study**

| name | sequence[a] | site |
|---|---|---|
| Nad-N2 | attcagatgcatTAAGACACGACACCGGCAGAATTG | NsiI |
| gpr-R | gattagcatgcCGGCATTAATATCTGTTAATATGTGC | SphI |
| Nad-N5 | attcagatgcatCTTTAATATGTAAACAAACTTGGTGG | NsiI |
| Nad-Sp | attcagcatgctacGCTCATTACCTTTGTGAGTGG | SphI |
| 1843-F | attcacatATGCCTACCCAATCAAAACATGCG | NdeI |
| 1843-R2 | attcatgcatCGGCGTATTACGAGTTCAACGCATCCTCG | NsiI |
| EryXbaF | attcgtctagaGCAAACTTAAGAGTGTGTTGATAG | XbaI |
| EryBamR | atatatggatccGGGACCTCTTTAGCTTCTTGG | *Bam*HI |
| R18A-F | CGGTCTGATACAGGCAgcGGAAGCCCTG | |
| R18A-R | CAGGGCTTCCgcTGCCTGTATCAGACCG | |
| W39A-F | CCGATCAGCAAgcGCGGATTATCCGTC | |
| W39A-R | GACGGATAATCCGCgcTTGCTGATCGG | |
| R40A-F | CCGATCAGCAATGGgcGATTATCCGTC | |
| R40A-R | GACGGATAATCgcCCATTGCTGATCGG | |
| Y115A-F | GTGGACGAACGCgcCGACGCTATCGAGG | |
| Y115A-R | CCTCGATAGCGTCGgcGCGTTCGTCCAC | |

[a]Capital letters and small letters indicate *N. meningitidis* derived sequences and sequences added for cloning purposes, respectively.

a GCG alanine codon and were used for transformation of the MC58-Δ1843 strain (Table 1). The resulting transformed strains were named MC58-Δ1843_CR18A, _CW39A, _CR40A, and _CY115A, respectively (Table 1). Total lysates from single colonies of all transformants were used as a template for PCR analysis to confirm the correct insertion by a double homologous recombination event. The *nadA* promoter was amplified and sequenced in each transformant to ensure


dx.doi.org/10.1021/bi300656w | *Biochemistry* 2012, 51, 6738−6752

that the same numbers of repeats were present as in the derivative strain. The *nadR* wild type or mutated genes in the complemented strains were expressed in an isopropyl β-D-1-thiogalactopyranoside (IPTG) inducible manner. A final concentration of 1 mM IPTG resulted in NadR expression levels similar to that of MC58 wild type strain.

**Site-Directed Mutagenesis - Protein Expression and Purification.** The sequence of *nadR* was mutated in the expression plasmid pET15-1843[8] as described above using the QuikChange II XL Site-Directed Mutagenesis kit (Stratagene) and the mutagenic primers pairs R18A-F/R18A-R, W39A-F/W39A-R, R40A-F/R40A-R, and Y115A-F/Y115A-R (Table 2). The resulting pET15-1843R18A, -1843W39A, -1843R40A, and -1843Y115A vectors were subsequently transformed into *Escherichia coli* BL21(DE3) strain for protein expression and purification (Table 1). Recombinant NadR proteins were purified as described previously.[8] Fractions containing the purified proteins were analyzed by SDS−PAGE, pooled, and dialyzed overnight against 50 mM Tris-HCl pH 8.0, 300 mM NaCl using a 10-kDa molecular weight cutoff dialysis membrane (Slide-A-lyzer dialysis cassettes, Pierce). The 6xHisTag was cleaved at room temperature using thrombin agarose resin (Sigma Aldrich) and removed with the Ni-NTA matrix. The purity and the identity of each protein were verified by SDS−PAGE and mass spectrometry, and the concentrations were measured using the Bradford assay. Purified proteins were aliquoted, flash frozen in ethanol/dry ice, and stored at −80 °C until use.

**Determination of the Oligomerization State of the Recombinant NadR Proteins.** Size-exclusion chromatography was performed on a ACQUITY UPLC ClassH system (Waters) using a Waters ACQUITY UPLC BEH200 SEC 1.7 μm column (4.6 × 150 mm) equilibrated at 30 °C with 10 column volumes of running buffer (50 mM sodium phosphate, pH 6.8, 300 mM NaCl). Two concentrations of each recombinant protein were tested in duplicate and the elution was performed with the running buffer at a flow rate of 0.35 mL/min. The elution profiles were recorded at 280 and 214 nm and analyzed with the Empower Pro software (Waters).

For native mass spectrometry, protein samples were buffer exchanged against 250 mM ammonium acetate (pH 8.0) using Zeba spin desalting columns with a 7-kDa molecular weight cutoff (Thermo Scientific). Samples (10 μM final) were analyzed on a SynaptG2 HDMS mass spectrometer (Waters) equipped with a nanoelectrospray source. The instrument was calibrated in resolution mode ($m/z$ 1000−7000) using a 100 mg/mL cesium iodide solution prepared in water, and the quadrupole profile was adjusted to ensure the best transmission in the selected mass range. Spectra were acquired in positive mode for 5 to 10 min to obtain a good signal-to-noise ratio and processed with MassLynx 4.1 software (Waters) with minimal smoothing.

**Sample Preparation for HDX-MS Analyses.** The labeling was initiated by dilution of the free and ligand-bound proteins with 10-fold 2.5 mM Tris (pD 8.0), 5 mM NaCl in 99.9% $D_2O$. In ligand binding experiments, the NadR proteins were preincubated with different ligand concentrations to test six protein/ligand ratios (mol/mol): 1/2, 1/10, 1/20, 1/100, 1/200, and 1/500, respectively. The ligand was allowed to incubate with the NadR proteins for 1 h at room temperature before the addition of the deuterated buffer. All exchange reactions were performed on ice, unless specified. Over the time course of the experiment (spanning from 30 s to 10 h), 5 μL of deuterated samples (20−40 pmol) were removed and quenched with 10 μL of an ice-cold 0.5% formic acid solution to lower the pH to 2.4. The quenched samples were immediately frozen in dry ice and stored at −80 °C for less than 24 h. A fully deuterated control was prepared as described above and left to incubate overnight at 37 °C.

**Global and Local HDX-MS Analyses − Data Processing.** Labeled samples were thawed rapidly to 0 °C and injected into a Shimadzu LC-20ADXR Prominence HPLC system controlled by a CMB-20A module. The injector, switching valve, columns, solvents, and all associated tubings were placed on ice to limit back-exchange. Blanks were run between samples to prevent carryover and abnormal back-exchange during LC separation.[27] For global HDX-MS, protein samples were trapped and desalted for 2 min at a flow rate of 220 μL/min using a Protein Micro Trap column (Michrom BioResources, Inc.) equilibrated with 100% buffer D (0.1% formic acid in water). Proteins were directly eluted into the mass spectrometer at a flow rate of 60 μL/min with 55% solvent E (acetonitrile/water (9/1), 0.1% formic acid).

Prior to local HDX-MS analysis, each protein sample was digested for 5 min on ice with a pepsin solution prepared in 0.4% formic acid, pH 2.4 (protein/pepsin ratio: 1/1, w/w). The generated peptides were loaded onto a Peptide Micro Trap column (Michrom BioResources, Inc.), desalted for 2 min at 220 μL/min with 5% buffer E, and separated on a Phenomenex C12 Jupiter Proteo reverse phase column (4 μm, 90 Å, 50 × 1.0 mm) with a linear gradient from 5 to 60% solvent E over 12 min at 50 μL/min. The last peptide was eluted from the column at $t$ = 8.5 min.

Mass spectra were acquired in resolution mode ($m/z$ 100−2000) on a Waters SynaptG2 mass spectrometer equipped with a standard ESI source. Mass accuracy was ensured by continuously infusing a GFP solution (600 fmol/μL in 50% acetonitrile, 0.1% formic acid) through the reference probe of the ESI source. The excel-based program HDX-Express[28] was used to extract the centroid mass of each peptic peptide as a function of the labeling time. The relative number of incorporated deuterons ($D$) was determined using the following equation:

$$D = \frac{m_t - m_{0\%}}{m_{100\%} - m_{0\%}}$$

where $m_t$ is the centroid mass value of the peptide at a specified exchange time $t$, and $m_{0\%}$ and $m_{100\%}$ correspond to the centroid mass of the undeuterated and the fully deuterated peptide, respectively. The average deuterium loss due to back-exchange was ∼25%. Since all experiments were conducted the same day and under identical conditions, the deuterium levels were not corrected for back-exchange and are reported as relative. The labeling kinetics of all peptides was fitted to a biexponential expression using Graphpad Prism 5.0 (GraphPad Software, San Diego California USA).

The identity of each peptide was confirmed by a combination of intact mass measurement, data-dependent MS/MS (DDA), and $MS^E$ analyses. Data were processed using Biopharmalynx 1.2 (Waters), and each fragmentation spectrum was manually inspected to confirm the assignment.

**Docking Experiments.** The coordinates of the 4-HPA molecule were obtained from the pdb Web site (ID numbers: 4HP). The AutoDockTools 1.5.4 (ADT) software was used to prepare the ligand for docking.[29] Briefly, the solvatation parameters and the Gasteiger charges were automatically


dx.doi.org/10.1021/bi300656w | *Biochemistry* 2012, 51, 6738−6752

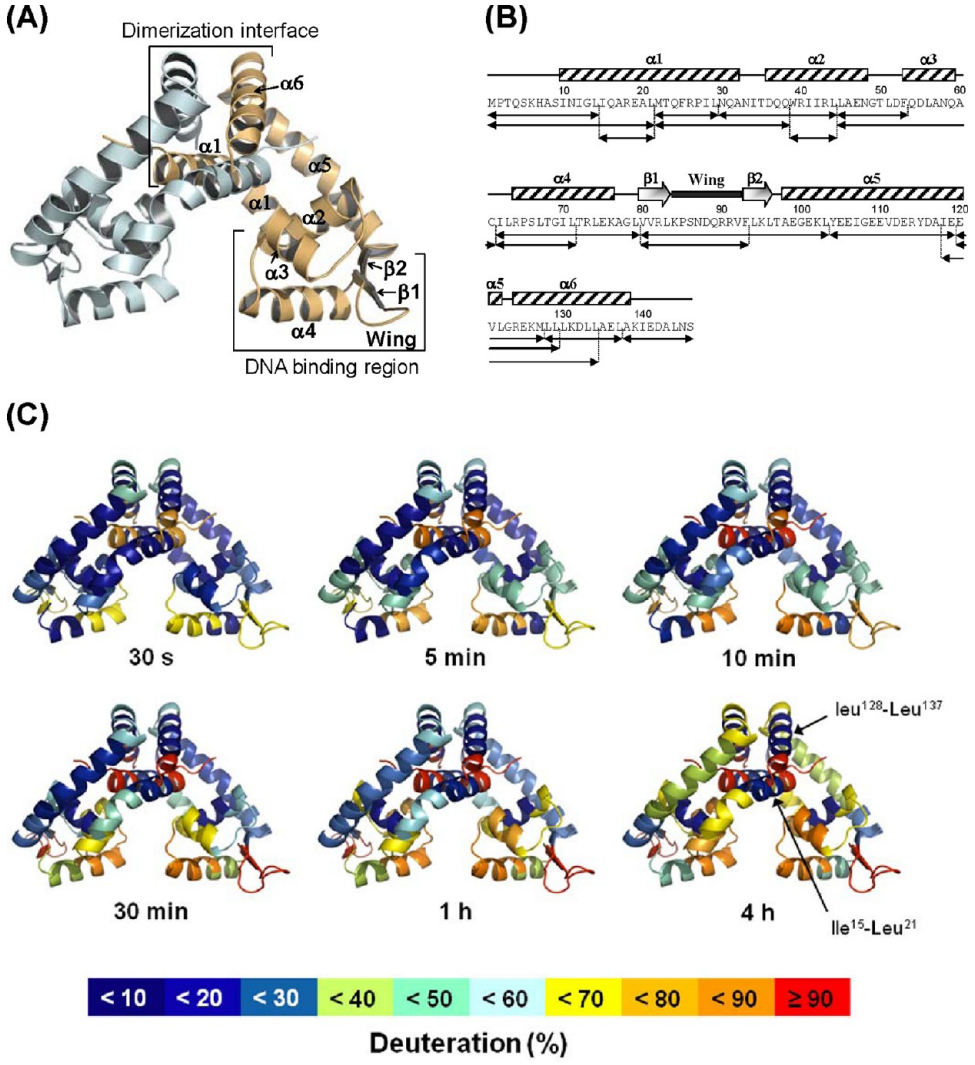


**Figure 2.** Homology model and dynamic analysis of NadR. (A) Ribbon representation of the proposed homodimeric structure of NadR obtained with SWISS-MODEL and based on the X-ray structure of a homologue regulator from *Pseudomonas aeruginosa* (PDB accession number: 2FBI).[36] One subunit is colored in gold and the other is in light blue. According to this model, each monomer adopts the typical fold of the MarR family members, which consists of six $\alpha$-helices and two-stranded $\beta$-sheets. The dimerization interface and the DNA-binding regions are indicated. (B) Sequence of NadR showing the 19 unique peptides used for HDX-MS analysis (100% sequence coverage). Secondary structure elements are reported above the sequence, following the structural model of NadR obtained with SWISS-MODEL (C). Dynamic analysis of NadR. The averaged percentage of deuterium uptake ($n$ = 3) of each individual peptide calculated after 30 s, 5 min, 10 min, 30 min, 1 and 4 h labeling is mapped onto the homology model of NadR. The color code is reported at the bottom of the figure.

added, and the torsional degrees of freedom of the molecule were estimated with AutoTors4, an additional module of ADT. The number of flexible torsions was set to 4. The structural model of NadR was prepared for docking experiments as follows: polar hydrogens and Gasteiger charges were added using ADT and the grid maps for each atom type found in 4-HPA were calculated with AutoGrid 4.0. For blind docking, the grid box was centered on the macromolecule, and the search parameters were set to enclose the entire homodimer using a 0.5 Å grid spacing. Results obtained by HDX-MS were directly used for data-directed docking experiments. The box size in the $x$-, $y$-, and $z$-axis was set to 45 × 55 × 45 points with a grid spacing of 0.375 Å. The center of the grid box was positioned just above the $\alpha$2 helix in order to surround the 4-HPA binding regions delineated by HDX-MS.

Docking experiments were performed with Autodock 4.0[29] using the Lamarckian genetic search algorithm and the default parameters. During the search process, the protein was regarded as rigid, while the ligands were regarded as being flexible. The number of docking runs was set to 10 for each docking experiment. The resulting docked conformations were clustered into families of similar conformations using a root mean squared deviation clustering tolerance of 0.5 Å.

**Western Blot Analysis.** Colonies from freshly grown overnight plate cultures were resuspended in GC medium to an $OD_{600}$ of 0.05 and grown at 37 °C to logarithmic phase ($OD_{600}$ of 0.5, ca. 2 h incubation). When indicated the growth was followed by 1 h induction at 37 °C with 1 mM IPTG and/or with 5 mM 4-HPA. One milliliter of each sample was resuspended in a defined volume of SDS−PAGE loading buffer to normalize cell density to a final $OD_{600}$ of 5. For Western blot analysis, 7 $\mu$L of each total protein sample was separated by SDS−PAGE and transferred onto a nitrocellulose filter by standard methods. Filters were blocked overnight at 4 °C by agitation in blocking solution (10% skim milk and 0.05% Tween 20 in PBS) and incubated for 1 h at 37 °C with primary


dx.doi.org/10.1021/bi300656w | *Biochemistry* 2012, 51, 6738−6752

antibodies (1:10000 anti-fHBP, 1:5000 anti-NadA, and 1:4000 anti-NadR) in 3% skim milk solution. After washing, the filters were incubated with a 1:2000 dilution of HRP-labeled antimouse (Dako) or antirabbit (Biorad) IgG in 3% skim milk solution for 1 h at room temperature. The resulting signal was detected with the Western Lightning-ECL chemiluminescent substrate (Perkin-Elmer).

**Electromobility Shift Assays (EMSA).** For EMSA experiments, two probes spanning from −170 to −116 (OpI) and −9 to +81 (OpII) with respect to the MC58 *nadA* promoter were amplified using Nad-N2/gpr-R and Nad-N5/Nad-Sp primer pairs respectively (Table 2). Two picomoles of DNA were radioactively labeled and used at the final concentration of 1.6 nM. The labeled probes were submitted to EMSA analysis with NadR WT or NadR mutant proteins (from 0 to 1215 ng diluted in protein solution [5 mM Tris-HCl pH 8, 60 mM NaCl]) as previously described,[8] with the following differences. The Gelshift binding buffer used was composed of 40 mM Tris-HCl pH 8, 5 mM $MgCl_2$, 50 mM KCl, 0.05% NP40, 10% glycerol with 30 nM salmon sperm DNA as nonspecific competitor. To assess the specificity of binding of NadR on the DNA labeled probes, 1.6 nM, 8 nM, and 40 nM (1-, 5-, or 25-fold respect to the probe) of either salmon sperm DNA or cold OpI and OpII DNAs were added as nonspecific or specific competitors, respectively. Where indicated, 5 or 10 mM 4-HPA was added to 100 ng of recombinant NadR WT or NadR mutant proteins in the binding reaction, to test the protein's responses to 4-HPA.

## RESULTS

**NadR Adopts a Homodimeric Organization in Solution.** It has been previously reported by footprinting experiments that NadR binds to and protects three distinct operators in the *nadA* promoter with a size compatible to a homodimeric organization.[8] To confirm the oligomerization state of NadR, the purified recombinant protein was subjected to a gel filtration analysis. As reported in Figure 1B, NadR was eluted from the column as a single and symmetric peak with a retention time corresponding to an estimated molecular weight of 36 kDa, thereby indicating that the purified protein adopts a homodimeric organization in solution. This result was further validated by nondenaturing nanoelectrospray mass spectrometry. The native mass spectrum of NadR at a final concentration of 10 $\mu$M showed an intense and well-resolved charge state series, from +8 to +16, in the 2100−4300 $m/z$ range (Figure 1C). The measured molecular weight (33727.8 ± 0.4 Da) was consistent with the expected mass of the dimer (33728.6 Da), therefore confirming that NadR, similar to other members of the MarR family, forms a noncovalent homodimer in solution.[16,18,30−35]

**Characterization of the Structural Model of NadR.** In order to aid HDX-MS data interpretation, a structural homology model of NadR was generated using the crystal structure of the transcriptional regulator PA4135 from *Pseudomonas aeruginosa*[36] which shares 42% sequence identities with NadR (Supplementary Figure S1). According to this model, the NadR dimer adopts the typical "triangle" shape of the MarR family with each monomer consisting of the secondary structure elements $\alpha$1-$\alpha$2-$\alpha$3-$\alpha$4-$\beta$1-wing-$\beta$2-$\alpha$5-$\alpha$6 (Figure 2A). The two monomers associate via a dimerization interface created by their N- and C-terminal helices ($\alpha$1, $\alpha$5, and $\alpha$6), and each monomer contains a winged helix-turn-helix (w-HTH) DNA-binding motif ($\alpha$3, $\alpha$4, $\beta$1, wing, $\beta$2).

The quality of our model was assessed by HDX-MS analysis.[37] The rate at which backbone amide hydrogens (NHs) exchange in solution is directly dependent on the dynamics and the structure of the protein.[38] Therefore, regions with secondary structures or occluded from the deuterated buffer will exchange more slowly than regions without any secondary structures and/or fully exposed to the solvent. To test our model, the average deuterium exchange behavior of 19 unique peptic peptides covering 100% of the NadR sequence (Figure 2B) was measured at specific time points and overlaid onto our structural model (Figure 2C). These data show that the core of the protein, including the dimerization interface ($\alpha$1, $\alpha$5, $\alpha$6) and $\alpha$2, is well protected from exchange with less than 20% incorporation after 30 min labeling. This result is in agreement with the high content of $\alpha$-helices present in each monomer and the function of $\alpha$1, $\alpha$5, and $\alpha$6 in the dimerization process. It is also interesting to note that the N-terminal part of $\alpha$1 (peptide $Ile^{15}$-$Leu^{21}$) and the C-terminal part of $\alpha$6 (peptide $Leu^{128}$-$Leu^{137}$) remain highly protected even after 4 h incubation (<10% incorporation). These two regions are predicted to be very close in our model and might interact together to generate the well-packed hydrophobic core of the dimer interface. In contrast to the dimerization interface, the w-HTH DNA-binding motif was found to be highly accessible. The N-terminal end of the recognition helix ($\alpha$4), as well as the two antiparallel $\beta$-strands ($\beta$1 and $\beta$2) and the wing exhibit fast initial exchange with more than 60% incorporation after 30 s incubation (Figure 2C). This is consistent with the fact that these regions must remain fully accessible and/or dynamic to interact with DNA.[21] Interestingly, two distinct exchange behaviors were observed in the recognition helix. While the N-terminal end of $\alpha$4 displays fast initial exchange, the C-terminal portion remains highly protected even after 10 min incubation. As reported in the BsOhrR/DNA complex, the N-terminal end of each recognition helix is directly introduced into one major groove of the DNA.[39] The observed difference of dynamics appears consistent with the DNA binding function of $\alpha$4. Indeed, the flexibility of the N-terminal end of $\alpha$4 might be required to correctly position the recognition helix in order to facilitate DNA interactions. Altogether, our HDX data correlate well with the homology-based structural model of NadR.

**4-HPA Binds at the Dimerization/DNA Interface.** To localize the 4-HPA biding pocket, the exchange behaviors of the apo- and HPA-bound forms were monitored and compared. The protein concentration was adjusted to 10 $\mu$M in the labeling buffer to prevent dimer dissociation. Global HDX-MS experiments were first carried out to measure the response of the protein to 4-HPA binding. After 1 h incubation, a total of 53 NHs were exchanged against deuterons in the apo-form, whereas the number of exchanged NHs was reduced to 48 in the presence of 4-HPA (Supplementary Figure S2). These results reveal that only a few NHs were protected upon complex formation, therefore indicating that the overall accessibility of the protein was similar in the presence and absence of ligand. To gain more detailed structural data and to localize the 4-HPA binding sites, the exchange behaviors of the free and HPA-bound states of NadR were compared after pepsin digestion. The cumulative error of measuring the deuterium incorporation in this experiment was ±0.12 Da using four independent replicates; any changes larger than that were considered significant when comparing the two data sets. Four regions, including $Met^{1}$-$Leu^{14}$ (N-term $\alpha$1), $Met^{22}$-$Leu^{29}$ (C-


dx.doi.org/10.1021/bi300656w | *Biochemistry* 2012, 51, 6738−6752

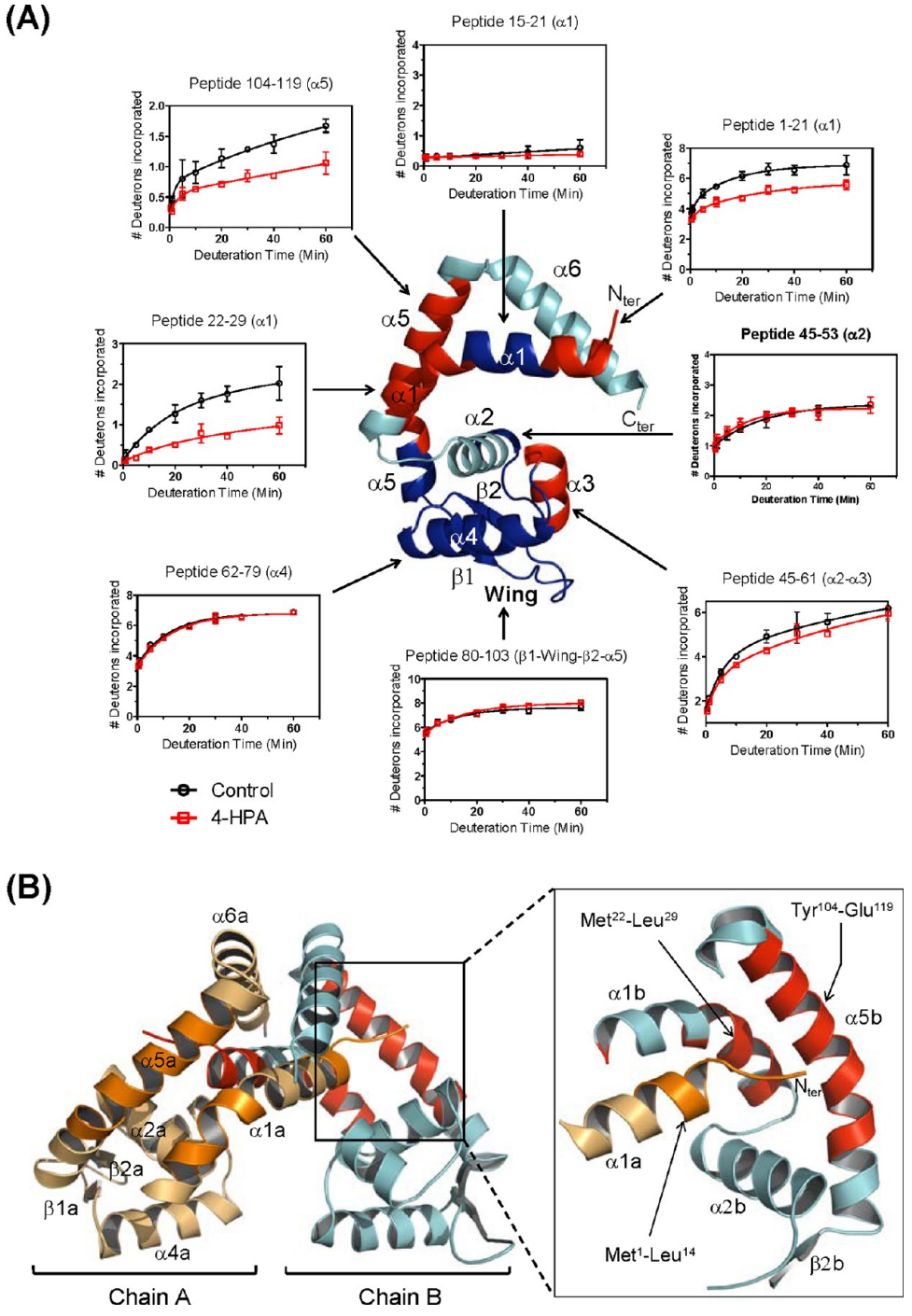


**Figure 3.** Local HDX-MS analysis of NadR in the absence and presence of 4-HPA. (A) Kinetic analysis of selected peptides upon 4-HPA binding. The relative number of incorporated deuterons in seven peptides of the protein [Met[1]-Leu[21] ($\alpha$1), Ile[15]-Leu[21] ($\alpha$1), Met[22]-Leu[29] ($\alpha$1), Leu[45]-Cys[61] (C-term $\alpha$2-$\alpha$3), Ile[62]-Leu[79] ($\alpha$4), Val[80]-Leu[103] ($\beta$1-Wing-$\beta$2-$\alpha$5), and Tyr[104]-Glu[119] ($\alpha$5)] is directly plotted onto the homology model of the NadR monomer. Specific regions of the protein showing reduced or no change of deuterium uptake upon ligand binding are colored in red and blue, respectively. The experiment was conducted four times. (B) Ribbon representation of NadR showing the position of the putative 4-HPA binding region identified by HDX-MS. Regions with altered deuterium uptake are colored in orange (chain A) and red (chain B). The solvent reduction observed in peptide Leu[45]-Cys[61] (C-term $\alpha$2-$\alpha$3) is omitted for clarity. The 4-HPA-binding pocket is located at the interface between the dimerization and the DNA-binding domains and is mainly formed by the $\alpha$1 N-terminal domain of chain A and the helices $\alpha$2, $\alpha$5, and the $\alpha$1 C-terminal domain of chain B (see expanded view).

term $\alpha$1), Asn[54]-Cys[61] ($\alpha$3), and Tyr[104]-Glu[119] ($\alpha$5), were protected from exchange upon 4-HPA binding (Figure 3A, red colored). To visualize more precisely our results, these regions were mapped onto the structural model of the dimer. Interestingly, with the exception of $\alpha$3, the reduction of solvent accessibility was clustered at the interface between the dimerization and the w-HTH DNA-binding domains (Figure 3B). This interface has already been identified as a common salicylate-binding pocket in several MarR homologues including MTH313,[22] ST1710,[21] SlyA,[40] and TcaR.[19] Although salicylate


dx.doi.org/10.1021/bi300656w | *Biochemistry* 2012, 51, 6738−6752

does not bind NadR, based on these observations, we conclude that 4-HPA likely shares the same protein binding region.

**Binding of 4-HPA Stabilizes the Homodimeric State of NadR.** The presence of salicylate was shown to stabilize the transcriptional regulator MTH313.[22] To address whether 4-HPA induces a similar effect on NadR, the dissociation of the dimer was monitored by global HDX-MS in the presence and absence of ligand. To promote dissociation, the dimer concentration was adjusted from 10 to 4 $\mu$M in the labeling buffer and the reaction was performed at room temperature. Using these experimental conditions, NadR incorporates the deuterium following a bimodal distribution indicative of EX1 kinetics[41,42] (Figure 4A, left panel). EX1-type exchange is a rare phenomenon and occurs when the refolding rate for a given segment of the protein is slower than the deuterium exchange rate, but several factors including oligomer dissociation during labeling may cause false EX1 signatures.[27] To prove that the EX1 signature arises from dissociation of the dimer, we analyzed the exchange pattern of each peptide after pepsin digestion. The EX1 signature was only observed on peptides located at the dimerization interface (i.e., $\alpha$1, $\alpha$5, and $\alpha$6) (Supplementary Figure S3). We conclude therefore that the bimodality arises from dissociation of the dimer; the lower and higher mass distributions observed in the mass spectra correspond respectively to the dimers that did not dissociate and to the dimers that did dissociate during labeling.

Confident that the dimer dissociates in these experimental conditions, the global HDX-MS analysis was repeated in the presence of 4-HPA. As shown in Figure 4A (right panel), the dissociation rate of the dimer was clearly slowed-down upon complex formation. To better quantify the effects of 4-HPA binding, the percentages of the higher mass species were extracted from each mass spectrum and plotted versus the labeling time to measure the dissociation rates. Compared to the apo-form, the HDX-MS derived dissociation rate of the dimer (0.023 $min^{-1}$) was reduced by a factor 4 (0.006 $min^{-1}$) upon complexation with 4-HPA, thereby indicating that the dimer was stabilized in the complex (Figure 4B). Moreover, the stabilization of the homodimeric state of NadR by 4-HPA was also confirmed by thermostability measurment by differential scanning calorimetry (data not shown).

**Identification of Key Residues in the 4-HPA Binding Pocket by in Silico Docking.** In an attempt to identify the residues of NadR in contact with 4-HPA, we used an *in silico* docking approach.[43] We first conducted a blind docking assay using the entire structure of the homodimer. The two predicted 4-HPA binding sites were both located at the junction between the dimerization and the DNA-binding domains and encompassed three regions identified by HDX-MS (Figure 5A). On the basis of the calculated docking energies, the first 4-HPA binding site (Figure 5A, purple) appears more favorable with a docking energy of −6.8 kcal·$mol^{-1}$ compared to −5.6 kcal·$mol^{-1}$ for the second site (Figure 5A, yellow). We next performed a second round of docking by restricting the search area to the regions identified by HDX-MS. As shown in Figure 5B, the 4-HPA molecule was nicely docked into a cavity mainly created by helices $\alpha$1 and $\alpha$5. The two best-ranked 4-HPA binding modes (denoted 1 and 2) along with their respective docking energies are presented in Figure 5C. Although the docking energies of 4-HPA-1 and 4-HPA-2 were identical, the orientation of the ligand in the binding pocket was radically different. In the first binding conformation, the hydroxy-phenyl group of 4-HPA practically faces $\alpha$5 and makes hydrogen bonds

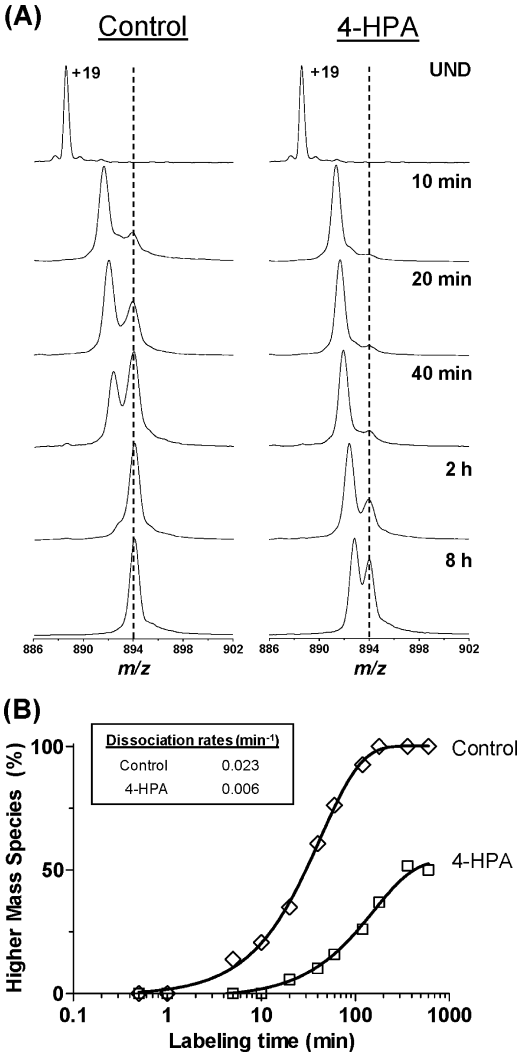


**Figure 4.** Binding of 4-HPA stabilizes the homodimeric form of NadR. (A) Mass spectra of the +19 charge state of NadR alone (control) or in the presence of a 200-fold molar excess 4-HPA. To promote the dissociation of the dimer, the protein concentration was adjusted to 4.7 $\mu$M in the deuterated buffer and the labeling performed at room temperature. Under these conditions, NadR incorporates the deuterium following a bimodal distribution (UND, undeuterated). The black dashed lines are provided for visual guidance. (B) Estimation of the dissociation rates of the homodimer in the free and bound state. The percentage of the NadR population having experienced at least one dissociation step (highly exchanged species) was determined by measuring the area-under-peak of the extracted ion current of the +19 charge state and plotted versus the exchange time. The reported dissociation rates of the homodimer correspond to the slopes of each curve.

with $Tyr^{115}$ ($\alpha$5) and $Arg^{43}$ ($\alpha$2), while the carboxylic acid moiety points toward $\alpha$1 to interact with $Arg^{18}$ ($\alpha$1) and $Arg^{40}$ ($\alpha$2). In the second binding conformation, the hydroxy-phenyl group points toward $\alpha$1 and interacts with $Arg^{40}$ ($\alpha$2), while the carboxylic group now faces helix $\alpha$5 and makes hydrogen bonds with $Trp^{39}$ ($\alpha$2) and $Arg^{43}$ ($\alpha$2). The predicted network of hydrogen bonds observed in the two 4-HPA binding modes mainly involves residues $Arg^{18}$, $Trp^{39}$, $Arg^{40}$, $Arg^{43}$, and $Tyr^{115}$ (Figure 5C). These residues were selected for mutagenesis to further determine their *in vivo* and *in vitro* functions in 4-HPA binding.


dx.doi.org/10.1021/bi300656w | *Biochemistry* 2012, 51, 6738−6752

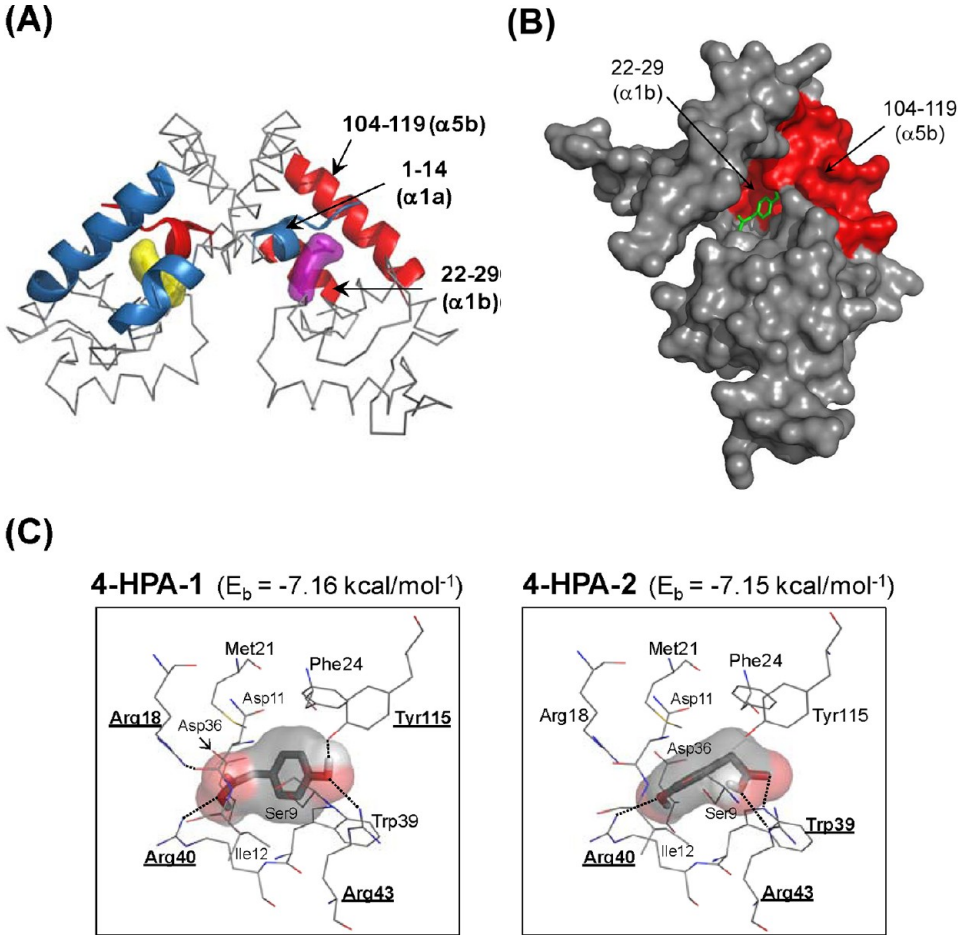


**Figure 5.** Identification of key residues in the 4-HPA binding pocket by molecular docking. (A) Results of the blind docking experiment performed with NadR and the 4-HPA. The grid box search parameters were set to enclose the entire homodimer. Two equivalent 4-HPA binding sites were identified at the interface between the dimerization and the DNA-binding domains (purple and yellow). Regions identified by HDX-MS with altered solvent accessibility upon ligand binding are also reported (cartoon representation) and colored in blue ($\alpha$1, monomer A) and red ($\alpha$1 and $\alpha$5, monomer B) respectively. The solvent reduction observed in peptide Leu$^{45}$-Cys$^{61}$ (C-term $\alpha$2-$\alpha$3) is omitted for clarity. (B) Surface model of the NadR monomer showing the best predicted 4-HPA binding mode obtained after data-directed docking experiment. The position of the 4-HPA binding site delineated by HDX-MS was used to center the grid box and to delimit the size of the search box. The molecule is docked into a pocket created at the junction between the dimer interface and the DNA-binding domains. Selected regions showing reduction of deuterium uptake upon 4-HPA binding are indicated in red. (C) Detailed representations of the two best-ranked binding conformations of 4-HPA with their respective binding energies ($E_b$). Residues predicted to be hydrogen-bonded [in bold type, underlined: Arg$^{18}$ ($\alpha$1), Trp$^{39}$ ($\alpha$1), Arg$^{40}$ ($\alpha$2), Arg$^{43}$ ($\alpha$3), and Tyr$^{115}$ ($\alpha$5)] or in close-contact to the docked 4-HPA molecule are represented as sticks and labeled in the figure.

**In Vivo 4-HPA Sensing of Selected Site Directed NadR Mutants.** In order to characterize the role of the selected residues in the *in vivo* response to 4-HPA, the previously described MC58-Δ1843 *nadR* null mutant strain[8] was complemented either by the wild type NadR protein or by the introduction of the desired alanine substituted forms of NadR. Note that NadR R43A was not included in this study since we failed to introduce the R43A substitution. Western Blot analyses of NadA expression were performed to assess the ability of each NadR proteins to repress *nadA* expression and respond to 4-HPA inducer. As reported in Figure 6A, NadR R18A and R40A are unable to repress *nadA* (compare lines 5 and 9 to lines 1 and 3) and mimic the behavior of the Δ1843 strain in the presence and absence of 4-HPA. These results suggest that both substitutions affect the ability of NadR to repress the *nadA* promoter, likely by preventing DNA binding.

The protein NadR W39A presents a lower expression level compared to wild type NadR (compare line 7 to lines 1 and 3) which indicates that the stability of the protein is compromised by the substitution. Possibly as a result, NadR W39A is unable to repress *nadA* expression *in vivo* and exhibits a behavior similar to that of the Δ1843 strain. Interestingly, the addition of 4-HPA increases the expression level of NadR W39A, thus suggesting that 4-HPA still interacts and stabilizes NadR W39A (compare lines 7 and 8).

In contrast to R18A, W39A, and R40A, the substitution of Tyr$^{115}$ by Ala does not compromise the *in vivo* repressive function of the protein. Interestingly, NadR Y115A represses more efficiently *nadA* than NadR WT thus suggesting that NadR Y115A acts as a hyper-repressor of NadA expression (compare line 11 to lines 1 and 3). Moreover, the addition of 4-HPA does not affect the repressive activity of NadR Y115A (compare line 11 to lines 2 and 4). Taken together, these data reveal that the Y115A substitution compromises the response of the protein *in vivo* to the 4-HPA inducer without abrogating its ability to repress *nadA*.

**In Vitro Characterization of the DNA- and 4-HPA Binding Activities of the Purified NadR Mutant Proteins.**


dx.doi.org/10.1021/bi300656w | *Biochemistry* 2012, 51, 6738−6752

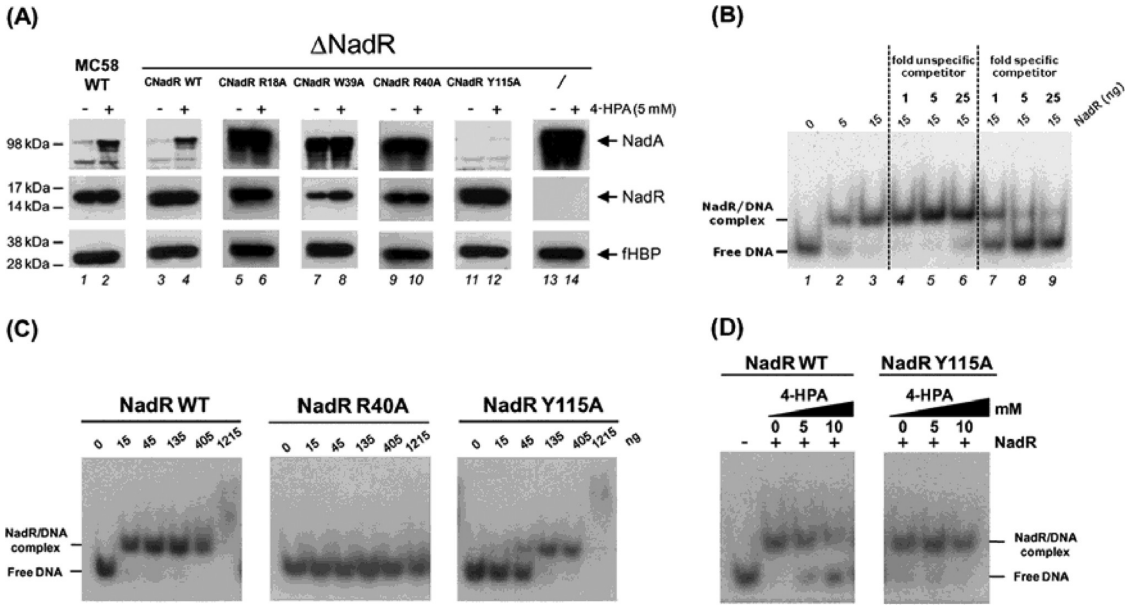


**Figure 6.** Substitution Y115A completely abolishes the in vivo and in vitro inhibitory effects of 4-HPA. (A) Western Blot analysis of the expression level of NadA and NadR in wild type MC58, *nadR* knockout MC58 (ΔNadR) and complemented ΔNadR strains. Cells recovered from an overnight culture on plates were grown in liquid media until midlog phase ($OD_{600}$ of 0.5) and then incubated for 1 h in the presence or absence of a fixed concentration of 4-HPA. Cells were harvested and 7 $\mu$L of total protein extract from each culture was subjected to SDS−PAGE and Western Blot analysis using anti-NadA, anti-NadR, or anti-fHBP antibodies as loading control. (B) Gel-mobility shift assays performed with a radioactively labeled DNA probe containing the individual OpI operator in the presence of increasing amounts of purified NadR WT (lines 1−3) and in the presence of either an increasing amount of a nonspecific competitor (salmon sperm DNA, lines 4−6) or a specific competitor (cold OpI DNA, lines 7−9). The positions of the free and complexed DNA are indicated. (C) Gel-mobility shift assays showing the binding activity of NadR WT, NadR R40A, and NadR Y115A on the OpI radio labeled probe. The R40A substitution completely abolishes the DNA-binding activity of NadR, while the Y115A substitution reduces the DNA-binding affinity. (D) Gel-mobility shift assay reporting the effects of 4-HPA on the OpI binding activity of NadR WT and NadR Y115A. The presence of increasing concentrations of 4-HPA only induces the release of the DNA probe from NadR WT.

To further elucidate the behavior of the NadR mutants, the recombinant proteins were expressed and purified from *E. coli* to assess their *in vitro* DNA-binding activity as well as their response to 4-HPA. With the exception of NadR W39A, the solubility and stability of NadR Y115A, R18A, and R40A were comparable to that of wild-type NadR. The instability of NadR W39A precludes its use and confirms that the functional defect observed *in vivo* likely results from disruption of the native structure of the protein (Figure 6A). The effects of each substitution on the structural integrity of NadR were investigated by gel filtration and global HDX-MS analysis. The mutant proteins were all dimeric in solution thus confirming that their oligomerization state was unaffected (Supplementary Figure S4). The extents of deuterium exchange of NadR Y115A and R40A were comparable to that of wild-type NadR indicating that their global folds were unaltered (data not shown). Surprisingly, NadR Y115A displayed a bimodal exchange pattern when diluted in the labeling buffer indicative of dimer dissociation (see next section below and Figure 7A). Given the fact that the dissociation of NadR Y115A occurs at a concentration in which the wild-type dimer is stable (i.e., 10 $\mu$M), these data suggest that $Tyr^{115}$ participates in the stabilization of the dimer. Finally, the R18A substitution significantly modifies the extent of deuterium incorporation suggesting that the structural integrity of the protein was compromised (Supplementary Figure S5).

To test the binding activity of the NadR proteins *in vitro*, we prepared a radiolabeled DNA probe containing the high affinity binding site OpI from the *nadA* promoter.[8] The binding specificity of NadR WT to the OpI labeled probe was first assessed by EMSA in the presence or absence of increasing amounts of either sonicated salmon sperm DNA (nonspecific competitor) or nonlabeled OpI DNA (specific competitor). As shown in Figure 6B (lines 1−3), a slow migrating complex is formed between NadR WT and the totality of the OpI labeled probe in the presence of 15 ng of protein. The addition of increasing amounts of the nonspecific competitor does not disrupt the complex (Figure 6B, lines 4−6), while the use of cold-OpI DNA prevents the binding of NadR WT to the radiolabeled OpI probe in a dose-dependent manner (Figure 6B, lines 7−9). This experiment demonstrates that NadR WT binds specifically to the OpI site of the *nadA* promoter. The same result was obtained using another labeled probe comprising the high affinity binding site OpII from the *nadA* promoter (data not shown).[8]

We next investigated the *in vitro* ability of NadR Y115A and R40A to bind to the OpI labeled probe. While NadR WT forms a DNA−protein complex with OpI, no interaction could be detected with NadR R40A even at high protein concentrations (Figure 6C). The DNA-binding activity of NadR R40A is abolished by the substitution indicating that $Arg^{40}$ is essential for DNA binding. Therefore, the *in vivo* defect of this mutant to repress NadA can be directly linked to its incapability to interact with the *nadA* promoter. In contrast to NadR R40A, the Y115A substitution does not abrogate the *in vitro* DNA-binding activity of the protein (Figure 6C). Interestingly, NadR Y115A binds OpI with a lower affinity compared to NadR WT. The apparent reduction of DNA-binding affinity contrasts with the *in vivo* hyper-repressive activity of NadR Y115A (Figure 6A) but could be explained by the effects of the substitution on


dx.doi.org/10.1021/bi300656w | *Biochemistry* 2012, 51, 6738−6752

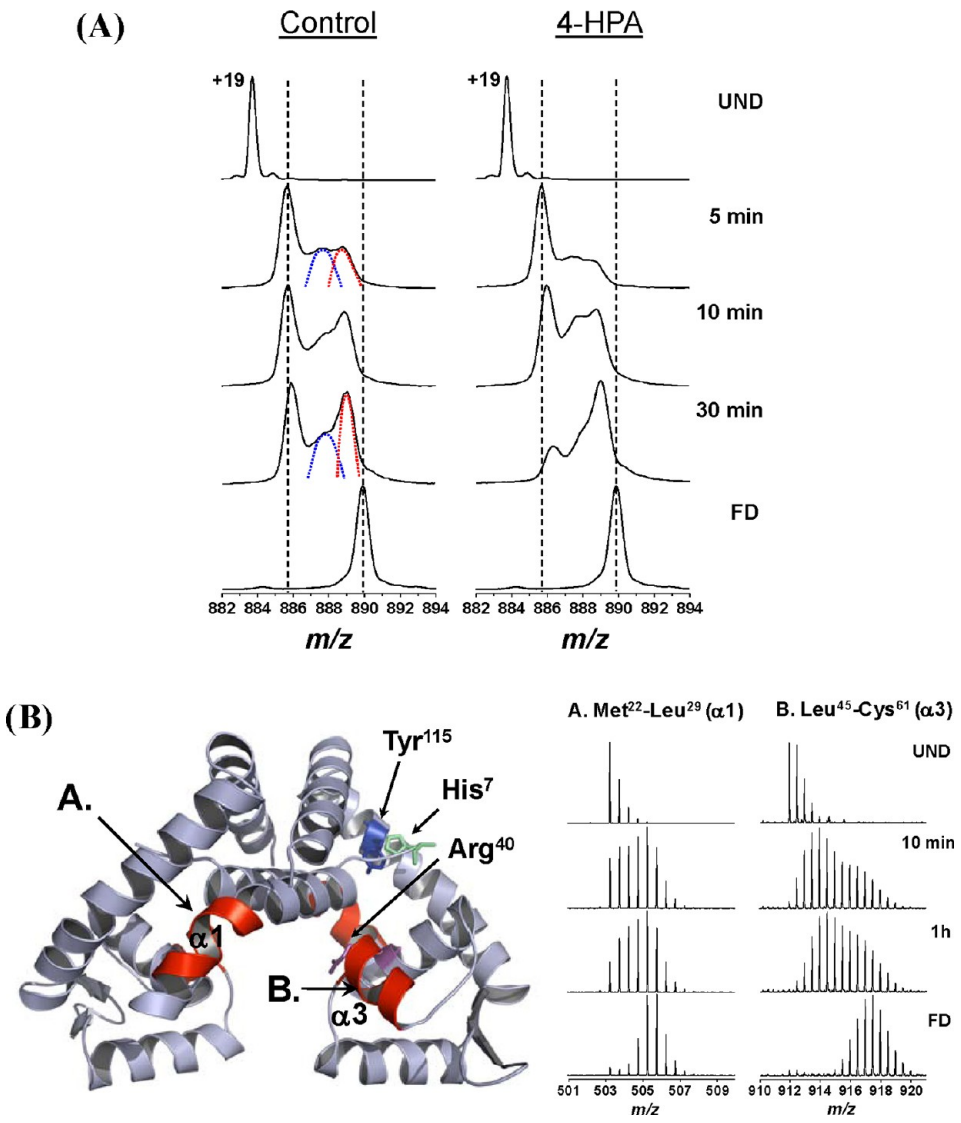


**Figure 7.** Substitution Y115A modifies the conformational/dynamic properties of elements located in helix $\alpha$1 and the DNA binding regions. (A) Mass spectra of the +19 charge state of NadR Y115A alone (control) or in the presence of a 200-fold molar excess 4-HPA. The labeling was performed using the same experimental conditions as the wild type protein (UND, undeuterated; FD, fully deuterated). Upon complex formation, a slight increase of deuterium uptake is observed along with an acceleration of the dissociation rate of the homodimer. The signal associated with the population of NadR Y115A that did dissociate during labeling (higher mass distribution) is indicated with the red dotted line. The intermediate mass distribution corresponding to a partially dissociated form of the dimer is indicated with blue dotted lines. The black dashed lines are provided for visual guidance. (B) The Y115A substitution modifies the isotopic distribution of peptides Met$^{22}$-Asn$^{38}$ (C terminus helix a1) and Leu$^{45}$-Cys$^{61}$ (helix $\alpha$3 of the DNA-binding region). The deuterium exchange pattern of the 2 peptides follows a bimodal distribution suggesting a change of dynamics. The location of the modified regions, along with the position of the mutated Tyr$^{115}$ (blue stick) and residue His$^{7}$ (orange stick) and Arg$^{40}$ (magenta stick), are reported onto the structural model of NadR. The bimodal patterns observed in peptides derived from the dimerization interface (i.e., peptides Ile$^{15}$-Leu$^{21}$ (N-terminus $\alpha$1), Leu$^{103}$-Glu$^{119}$ ($\alpha$5), and Leu$^{128}$-Leu$^{137}$ ($\alpha$6); see Supplementary Figure S2) are omitted for clarity.

the dimerization process (discussed below). Since the substitution modifies the *in vitro* stability of the dimer and MarR homologues bind DNA as dimers, higher NadR Y115A concentrations might be required compared to wild-type to stabilize the dimer and promote DNA binding.

Finally, the addition of 4-HPA does not disrupt the NadR Y115A/DNA complex even at 10 mM concentration (Figure 6D). Taken together, these data demonstrate that NadR Y115A is "blind" to the 4-HPA molecule.

**4-HPA Binding to NadR Y115A Accelerates the in Vitro Dissociation Rate of the Dimer.** NadR Y115A represents the only functional mutant unable to respond to 4-HPA. The absence of response to 4-HPA could be due to a failure of the ligand to interact with NadR Y115A. An alternative explanation is that 4-HPA is still able to interact with the protein but its binding is not sufficient to promote DNA dissociation. To determine whether Y115A affects the *in vitro* ability of NadR to bind 4-HPA, we measured and compared the deuterium exchange profiles of the protein in the absence and presence of ligand. As reported above, we found that Y115A affects the *in vitro* stability of the dimer (Figure 7A). This indicates that Tyr$^{115}$ plays a role in the dimerization process. Indeed, the side chain of Tyr$^{115}$ appears close enough to interact with residue His$^{7}$ thus allowing direct contact between helix $\alpha$5 of the first monomer and the $\alpha$1 N-terminal end of its counterpart (Figure 7B and Supplementary Figure


dx.doi.org/10.1021/bi300656w | *Biochemistry* 2012, 51, 6738−6752

S6). Surprisingly, in addition to the dimerization interface, the C-terminus of helix $\alpha$1 (peptide Met$^{22}$-Asn$^{38}$) and helix $\alpha$3 of the DNA-binding domain (peptide Leu$^{45}$-Lys$^{61}$) displayed a bimodal signature (Figure 7B). The substitution of residue Tyr$^{115}$ in the HPA-binding pocket modifies therefore the dynamics of specific regions located far from the mutation site which suggests that a communication network exists between elements of the HPA- and the DNA-binding domains.

We next performed the labeling with an excess of 4-HPA ligand. In addition to the lower and higher mass distributions, an intermediate mass distribution was observed in the mass spectra (Figure 7A, blue dotted lines). As recently reported by Engen and co-workers, sample carryover during LC separation at 0 °C can lead to abnormal back-exchange and artifactual lower mass distributions.[27] In this situation, the labeled protein that remains in the column during the first injection, and then elutes during the gradient in the second injection, is exposed to the LC buffer much longer than the second sample and loses more deuterium. To eliminate potential carryover, blank injections were run between samples. This washing procedure did not eliminate the intermediate mass population indicating that it was not an experimental artifact. Interestingly, the intermediate mass distribution was not observed after labeling at room temperature. Consequently, we believe that this population corresponds to a partially dissociated form of the dimer that is trapped during labeling at 4 °C. On the basis of our *in vivo* and EMSA results, one would expect that the substitution abolishes 4-HPA binding. However, the presence of the ligand accelerates the dissociation rate of the dimer (Figure 7A). In addition to this, a slight increase of deuterium uptake was observed (~4 Da at the 30 min time point). Detailed measurements of HDX in the presence of 4-HPA localize the increase of incorporation in helix $\alpha$3 (peptide Leu$^{45}$-Lys$^{61}$, see Supplementary Figure S7) suggesting a change in conformation or in dynamics. Altogether, these data indicate that the ligand still interacts with NadR Y115A and contrast with our EMSA results. Indeed, 4-HPA is unable to promote the *in vitro* dissociation of the protein/DNA complex which indicates that the effects of 4-HPA on the dimer dissociation rate are not sufficient to abolish DNA-binding. This result is surprising as MarR homologues only bind DNA as dimers. One possible explanation could be that NadR Y115A forms a very stable complex with DNA. As observed *in vivo*, NadR Y115A acts as a hyper-repressor of NadA expression compared to wild type meaning that, when bound to DNA, the protein does not dissociate (no basal expression level, Figure 6A). On the basis of these observations, it seems plausible that 4-HPA binding cannot counterbalance the stabilization effect induced by DNA. Altogether, these data reveal that Tyr$^{115}$ plays a key role in the mechanism of regulation of NadR by 4-HPA.

## DISCUSSION

NadR was recently identified as the negative transcriptional regulator of the adhesin/invasin NadA in Nm, an important virulence factor required for colonization and invasion of the mucosa.[9] The *in vitro* DNA-binding activity of NadR was shown to be attenuated by 4-HPA,[8] a catabolite of aromatic amino acids present in human saliva, and by human saliva itself,[14] thereby indicating that this molecule could act as an inducer of *nadA* expression *in vivo* during Nm infection. In this study, we have explored at the dynamic level the mechanism by which this molecule regulates the DNA-binding activity of NadR. Our results combined with our homology model allow us to draw some important conclusions and provide information on the effects of 4-HPA binding on the dynamics of the protein.

The 4-HPA ligand binds in a pocket located at the junction between the dimerization interface and the DNA-binding lobe. Our HDX-MS results reveal that the ligand binding site is mainly formed by structural elements of the two monomers including helix $\alpha$1 of the first subunit and helices $\alpha$1 and $\alpha$5 of the second subunit. Although the number of salicylate sites on MarR molecules is still controversial, superimposition of the NadR/4-HPA complex with available representative MarR/salicylate structures shows that 4-HPA shares a salicylate binding region common to all available models (Supplementary Figure S8).[19,22] The position of the ligand binding pocket appears therefore well conserved among MarR family members. However the ligand binding site of NadR displays significant variations in amino acid composition compared to other representative MarR homologues, which suggests differences in ligand specificity. Indeed, NadR does not respond to the broad specific effector salicylate *in vitro*[8] and is unable to associate with the ligand even at high concentrations (our unpublished results). These observations suggest that members of this family have probably evolved separately to respond to distinct signaling molecules thus enabling bacteria to adapt and respond to changing environmental conditions within their natural niches.

The presence of this conserved ligand binding pocket has led to the hypothesis of a shared mechanism of regulation among members of the MarR family. For proteins that appear to be preconfigured for DNA binding in their apo configuration, the binding of ligands produces a large conformational change that is transmitted to the DNA binding lobes.[22] The distance between the two recognition helices that is essential for association with two consecutive DNA major grooves is altered in the complex thus precluding DNA binding. For some homologues, however, the apo configuration does not appear to be compatible for DNA binding, and conformational changes are required to promote association with DNA.[19−21] In this case, the ligands likely regulate the DNA binding activity by stabilizing the protein in its apo configuration, as observed with ST1710 and TcaR. Compared to the first model, this mechanism of ligand-mediated regulation is associated with more subtle conformational changes. The binding of salicylate to TcaR drives an asymmetric conformational change in the w-HTH domain that modifies the orientation of helices $\alpha$3 and $\alpha$4 and blocks the DNA-binding lobes in a position incompatible for DNA binding.[19] In contrast, the structure of the salicylate/ST1710 complex appears very similar to the apo form with only minor conformational changes in the wings. Although no modifications were observed in helices $\alpha$3 and $\alpha$4, the authors believe that salicylate might induce a dynamic or allosteric change in ST1710 that would not be captured by crystallization.[21]

The formation of the 4-HPA/NadR complex results in the protection of a few backbone amide hydrogens compared to the apo form which reveals that the overall accessibility of the protein is similar in the presence and absence of ligand. With the exception of helix $\alpha$3, the exchange behavior of the recognition helix $\alpha$4 as well as the wings remains unaltered in the complex which indicates that 4-HPA likely regulates the DNA-binding activity of NadR without inducing large conformational changes in the DNA-binding lobes. In addition, our HDX-MS results reveal that the ligand affects the


dx.doi.org/10.1021/bi300656w | *Biochemistry* 2012, 51, 6738−6752

monomer−dimer equilibrium by stabilizing the homodimeric state of NadR. The 4-HPA-induced stabilization of the dimer is likely mediated by formation of additional contacts within the dimerization interface. Indeed, the $\alpha$1 N-terminal domain of the first monomer, which is deeply inserted between helices $\alpha$5 and $\alpha$6 of the second subunit, incorporates less deuterons in the presence of 4-HPA indicative of reduced solvent accessibility and/or increased hydrogen bonding (Figure 3). The 4-HPA ligand may therefore act as "glue" within its binding pocket by holding the $\alpha$1 N-terminal ends of each subunit in place thus creating additional anchoring points between the two monomers. Altogether, these data indicate that 4-HPA probably locks NadR in a conformation incompatible with DNA binding without inducing large conformational changes in the DNA-binding regions. On the basis of these observations, it is tempting to speculate that the apo configuration of NadR is not preconfigured for DNA binding. In this context, the binding of 4-HPA would prevent the conformational changes required for DNA binding, as seen for ST1710 and TcaR.[19,21]

In addition, the binding of 4-HPA slightly reduces the solvent accessibility of helix $\alpha$3 suggesting that 4-HPA induces minor conformational changes in the DNA-binding lobes. This hypothesis is further supported by our mutagenesis experiments. The substitution of $Tyr^{115}$ in the ligand binding site alters the dynamics of helix $\alpha$3 (and of the C-terminus of helix $\alpha$1) suggesting a cross-talk between elements of the HPA- and the DNA-binding domains. Although $Tyr^{115}$ was predicted to be in contact with 4-HPA by in *silico docking*, its substitution does not prevent ligand binding. Indeed, 4-HPA still modifies the exchange behavior of $\alpha$3 and accelerates the dimer dissociation rate. The presence of the ligand seems therefore to be not only transmitted to the DNA-binding domain ($\alpha$3) but also to the dimerization interface. It is well established that members of the MarR family possess an intrinsic conformational flexibility at the dimerization interface that is exploited on binding of either cognate DNA or ligand to modify the position of the DNA-binding domains.[6,7] On the basis of these observations, it is tempting to speculate that 4-HPA makes use of the structural malleability of the dimerization interface to alter the position of the DNA-binding lobes. However, such conformational changes would affect the global solvent accessibility of the whole DNA-binding lobes in the 4-HPA/NadR complex which appears inconsistent with our labeling data. It seems more plausible that 4-HPA reduces the flexibility of the dimerization interface to prevent the motions of the DNA-binding lobes required for interaction with DNA. On the basis of this model, the binding of the ligand may lock the DNA-binding lobes in place without affecting their global solvent accessibility. Finally, our mutagenesis data reveal that $Tyr^{115}$ plays a key role in the mechanism of regulation of NadR by 4-HPA. The Y115A substitution compromises the 4-HPA-mediated stabilization of the complex and prevents DNA dissociation. Taken together, these data suggest that 4-HPA makes use of $Tyr^{115}$ to lock the dimer in a conformation incompatible with DNA binding.

The mechanism of regulation of NadR by 4-HPA deduced from our data mainly relies on the stabilization of the dimer in a configuration incompatible with DNA binding. The binding of 4-HPA in its binding pocket may lock the position of the DNA-binding lobes in place by acting as a "glue" between the dimerization and the DNA-binding domains, thus preventing conformational changes required for DNA interaction. The model proposed above is based on the comparison of our HDX and mutagenesis data with available structural models of regulation of MarR homologues. The resolution of the crystal structure of NadR in its free and ligand-bound state would greatly facilitate our understanding of the mechanism of regulation of NadR by 4-HPA.

NadR has been recently demonstrated to regulate a regulon of genes in response to 4-HPA.[14] In this sense, the 4-HPA molecule could be seen as a signal used by Nm to adapt different cell functions to the host niche environment. However, we cannot exclude that NadR might also respond to other relevant physiological signals in different niches during infection. Indeed, we found that the 3-HPA molecule, a rutin metabolite present in human urine,[44,45] was also able to interact with NadR and to induce *nadA* expression *in vivo* (data not shown). Although 3-HPA has never been detected in saliva, these observations suggest that other molecules might interact with NadR and regulate its DNA-binding activity, as reported for other MarR homologues.[7] The identification of the 4-HPA binding pocket represents a good starting point for the discovery of other specific host niche signals with the capability to control the DNA-binding activity of NadR.

## ■ ASSOCIATED CONTENT

### Ⓢ Supporting Information

Figure S1: Sequence alignment between NadR and the transcriptional regulator PA4135 from *Pseudomonas aeruginosa*; Figure S2: HDX-MS analysis of peptides $Ile^{15}$-$Leu^{21}$ ($\alpha$1), $Tyr^{104}$-$Leu^{119}$ ($\alpha$5), and $Leu^{128}$-$Leu^{137}$ ($\alpha$6) located in the dimerization interface of NadR; Figure S3: Global HDX-MS analysis of NadR in the absence and presence of 4-HPA; Figure S4: Size exclusion chromatograms of NadR WT (control), NadR R18A, NadR R40A, and NadR Y115A; Figure S5: Global time course of deuterium incorporation of NadR WT and NadR R18A; Figure S6: Ribbon representations of NadR showing the position of residues $His^{7}$ ($\alpha$1a) and $Tyr^{115}$ ($\alpha$5b); Figure S7: Substitution Y115A modifies the exchange behavior and the level of deuterium incorporation of peptide Leu45-Lys61 (helix $\alpha$3) in the presence of 4-HPA; Figure S8: Comparison of the 4-HPA/NadR complex with representative MarR/salicylate structures. This material is available free of charge via the Internet at http://pubs.acs.org.

## ■ AUTHOR INFORMATION

### Corresponding Author

*Tel: +39 0577 539027. Fax: +39 0577 249314. E-mail: nathalie.norais@novartis.com.

### Notes

The authors declare no competing financial interest.

## ■ ACKNOWLEDGMENTS

We thank Dr. Simone Vecchi (Novartis Vaccines and Diagnostics, Siena) for his help with the ACQUITY UPLC ClassH system and Giorgio Corsi for artwork. L.F. and D.D. are the recipients of a Novartis fellowship from the Ph.D. program in Functional Biology of Molecular and Cellular Systems of the University of Bologna and from the Ph.D. program in Cellular, Molecular and Industrial Biology of the University of Bologna, respectively.

## ■ ABBREVIATIONS USED

Nm, *Neisseria meningitidis*; NadA, Neisserial adhesin A; NadR, Neisserial adhesin regulator; MarR, multiple antibiotic

resistance regulator superfamily; 4-HPA, 4-hydroxyphenylacetic acid; ADT, AutoDockTools; HDX-MS, hydrogen/deuterium exchange-mass spectrometry; ESI, electrospray ionization; DDA, data dependent acquisition; IPTG, isopropyl β-D-1-thiogalactopyranoside; EMSA, electromobility shift assay; OpI and OpII, operator I and II

## REFERENCES


(1) Cartwright, K. A., Stuart, J. M., Jones, D. M., and Noah, N. D. (1987) The Stonehouse survey: nasopharyngeal carriage of meningococci and Neisseria lactamica. *Epidemiol. Infect. 99*, 591−601.

(2) Rosenstein, N. E., Perkins, B. A., Stephens, D. S., Popovic, T., and Hughes, J. M. (2001) Meningococcal disease. *N. Engl. J. Med. 344*, 1378−1388.

(3) Dietrich, G., Kurz, S., Hubner, C., Aepinus, C., Theiss, S., Guckenberger, M., Panzner, U., Weber, J., and Frosch, M. (2003) Transcriptome analysis of Neisseria meningitidis during infection. *J. Bacteriol. 185*, 155−164.

(4) Echenique-Rivera, H., Muzzi, A., Del Tordello, E., Seib, K. L., Francois, P., Rappuoli, R., Pizza, M., and Serruto, D. (2011) Transcriptome analysis of Neisseria meningitidis in human whole blood and mutagenesis studies identify virulence factors involved in blood survival. *PLoS Pathog. 7*, e1002027.

(5) Ellison, D. W., and Miller, V. L. (2006) Regulation of virulence by members of the MarR/SlyA family. *Curr. Opin. Microbiol. 9*, 153−159.

(6) Perera, I. C., and Grove, A. (2010) Molecular mechanisms of ligand-mediated attenuation of DNA binding by MarR family transcriptional regulators. *J. Mol. Cell. Biol. 2*, 243−254.

(7) Wilkinson, S. P., and Grove, A. (2006) Ligand-responsive transcriptional regulation by members of the MarR family of winged helix proteins. *Curr. Issues Mol. Biol. 8*, 51−62.

(8) Metruccio, M. M., Pigozzi, E., Roncarati, D., Berlanda Scorza, F., Norais, N., Hill, S. A., Scarlato, V., and Delany, I. (2009) A novel phase variation mechanism in the meningococcus driven by a ligand-responsive repressor and differential spacing of distal promoter elements. *PLoS Pathog. 5*, e1000710.

(9) Schielke, S., Huebner, C., Spatz, C., Nagele, V., Ackermann, N., Frosch, M., Kurzai, O., and Schubert-Unkmeir, A. (2009) Expression of the meningococcal adhesin NadA is controlled by a transcriptional regulator of the MarR family. *Mol. Microbiol. 72*, 1054−1067.

(10) Bambini, S., Muzzi, A., Olcen, P., Rappuoli, R., Pizza, M., and Comanducci, M. (2009) Distribution and genetic variability of three vaccine components in a panel of strains representative of the diversity of serogroup B meningococcus. *Vaccine 27*, 2794−2803.

(11) Giuliani, M. M., Adu-Bobie, J., Comanducci, M., Arico, B., Savino, S., Santini, L., Brunelli, B., Bambini, S., Biolchi, A., Capecchi, B., Cartocci, E., Ciucchi, L., Di Marcello, F., Ferlicca, F., Galli, B., Luzzi, E., Masignani, V., Serruto, D., Veggi, D., Contorni, M., Morandi, M., Bartalesi, A., Cinotti, V., Mannucci, D., Titta, F., Ovidi, E., Welsch, J. A., Granoff, D., Rappuoli, R., and Pizza, M. (2006) A universal vaccine for serogroup B meningococcus. *Proc. Natl. Acad. Sci. U. S. A. 103*, 10834−10839.

(12) Pizza, M., Scarlato, V., Masignani, V., Giuliani, M. M., Arico, B., Comanducci, M., Jennings, G. T., Baldi, L., Bartolini, E., Capecchi, B., Galeotti, C. L., Luzzi, E., Manetti, R., Marchetti, E., Mora, M., Nuti, S., Ratti, G., Santini, L., Savino, S., Scarselli, M., Storni, E., Zuo, P., Broeker, M., Hundt, E., Knapp, B., Blair, E., Mason, T., Tettelin, H., Hood, D. W., Jeffries, A. C., Saunders, N. J., Granoff, D. M., Venter, J. C., Moxon, E. R., Grandi, G., and Rappuoli, R. (2000) Identification of vaccine candidates against serogroup B meningococcus by whole-genome sequencing. *Science 287*, 1816−1820.

(13) Serruto, D., Spadafina, T., Ciucchi, L., Lewis, L. A., Ram, S., Tontini, M., Santini, L., Biolchi, A., Seib, K. L., Giuliani, M. M., Donnelly, J. J., Berti, F., Savino, S., Scarselli, M., Costantino, P., Kroll, J. S., O'Dwyer, C., Qiu, J., Plaut, A. G., Moxon, R., Rappuoli, R., Pizza, M., and Arico, B. (2010) Neisseria meningitidis GNA2132, a heparin-binding protein that induces protective immunity in humans. *Proc. Natl. Acad. Sci. U. S. A. 107*, 3770−3775.

(14) Fagnocchi, L., Pigozzi, E., Scarlato, V., and Delany, I. (2012) In the NadR regulon, adhesins and diverse meningococcal functions are regulated in response to signals in human saliva. *J. Bacteriol. 194*, 460−474.

(15) Schielke, S., Spatz, C., Schwarz, R. F., Joseph, B., Schoen, C., Schulz, S. M., Hubert, K., Frosch, M., Schubert-Unkmeir, A., and Kurzai, O. (2011) Characterization of FarR as a highly specialized, growth phase-dependent transcriptional regulator in Neisseria meningitidis. *Int. J. Med. Microbiol. 301*, 325−333.

(16) Nichols, C. E., Sainsbury, S., Ren, J., Walter, T. S., Verma, A., Stammers, D. K., Saunders, N. J., and Owens, R. J. (2009) The structure of NMB1585, a MarR-family regulator from Neisseria meningitidis. *Acta Crystallogr. Sect. F Struct. Biol. Cryst. Commun. 65*, 204−209.

(17) Providenti, M. A., and Wyndham, R. C. (2001) Identification and functional characterization of CbaR, a MarR-like modulator of the cbaABC-encoded chlorobenzoate catabolism pathway. *Appl. Environ. Microbiol. 67*, 3530−3541.

(18) Alekshun, M. N., Levy, S. B., Mealy, T. R., Seaton, B. A., and Head, J. F. (2001) The crystal structure of MarR, a regulator of multiple antibiotic resistance, at 2.3 Å resolution. *Nat. Struct. Biol. 8*, 710−714.

(19) Chang, Y. M., Jeng, W. Y., Ko, T. P., Yeh, Y. J., Chen, C. K., and Wang, A. H. (2010) Structural study of TcaR and its complexes with multiple antibiotics from *Staphylococcus epidermidis*. *Proc. Natl. Acad. Sci. U. S. A. 107*, 8617−8622.

(20) Dolan, K. T., Duguid, E. M., and He, C. (2011) Crystal structures of SlyA protein, a master virulence regulator of Salmonella, in free and DNA-bound states. *J. Biol. Chem. 286*, 22178−22185.

(21) Kumarevel, T., Tanaka, T., Umehara, T., and Yokoyama, S. (2009) ST1710-DNA complex crystal structure reveals the DNA binding mechanism of the MarR family of regulators. *Nucleic Acids Res. 37*, 4723−4735.

(22) Saridakis, V., Shahinas, D., Xu, X., and Christendat, D. (2008) Structural insight on the mechanism of regulation of the MarR family of proteins: high-resolution crystal structure of a transcriptional repressor from Methanobacterium thermoautotrophicum. *J. Mol. Biol. 377*, 655−667.

(23) Takahama, U., Imamura, H., and Hirota, S. (2009) Nitration of the salivary component 4-hydroxyphenylacetic acid in the human oral cavity: enhancement of nitration under acidic conditions. *Eur. J. Oral Sci. 117*, 555−562.

(24) Takahama, U., Oniki, T., and Murata, H. (2002) The presence of 4-hydroxyphenylacetic acid in human saliva and the possibility of its nitration by salivary nitrite in the stomach. *FEBS Lett. 518*, 116−118.

(25) Sambrook, J., Fritsch, E. F., Maniatis, T. (1989) *Molecular Cloning: A Laboratory Manual*, 2nd ed., Cold Spring Harbor Laboratory, Cold Spring Harbor, NY.

(26) Ieva, R., Alaimo, C., Delany, I., Spohn, G., Rappuoli, R., and Scarlato, V. (2005) CrgA is an inducible LysR-type regulator of Neisseria meningitidis, acting both as a repressor and as an activator of gene transcription. *J. Bacteriol. 187*, 3421−3430.

(27) Fang, J., Rand, K. D., Beuning, P. J., and Engen, J. R. (2011) False EX1 signatures caused by sample carryover during HX MS analyses. *Int. J. Mass Spectrom. 302*, 19−25.

(28) Weis, D. D., Engen, J. R., and Kass, I. J. (2006) Semi-automated data processing of hydrogen exchange mass spectra using HX-Express. *J. Am. Soc. Mass Spectrom. 17*, 1700−1703.

(29) Morris, G. M., Huey, R., Lindstrom, W., Sanner, M. F., Belew, R. K., Goodsell, D. S., and Olson, A. J. (2009) AutoDock4 and AutoDockTools4: Automated docking with selective receptor flexibility. *J. Comput. Chem. 30*, 2785−2791.

(30) Bordelon, T., Wilkinson, S. P., Grove, A., and Newcomer, M. E. (2006) The crystal structure of the transcriptional regulator HucR from Deinococcus radiodurans reveals a repressor preconfigured for DNA binding. *J. Mol. Biol. 360*, 168−177.

(31) Di Fiore, A., Fiorentino, G., Vitale, R. M., Ronca, R., Amodeo, P., Pedone, C., Bartolucci, S., and De Simone, G. (2009) Structural analysis of BldR from Sulfolobus solfataricus provides insights into the

molecular basis of transcriptional activation in archaea by MarR family proteins. *J. Mol. Biol. 388*, 559−569.
(32) Lim, D., Poole, K., and Strynadka, N. C. (2002) Crystal structure of the MexR repressor of the mexRAB-oprM multidrug efflux operon of Pseudomonas aeruginosa. *J. Biol. Chem. 277*, 29253−29259.
(33) Newberry, K. J., Fuangthong, M., Panmanee, W., Mongkolsuk, S., and Brennan, R. G. (2007) Structural mechanism of organic hydroperoxide induction of the transcription regulator OhrR. *Mol. Cell 28*, 652−664.
(34) Poor, C. B., Chen, P. R., Duguid, E., Rice, P. A., and He, C. (2009) Crystal structures of the reduced, sulfenic acid, and mixed disulfide forms of SarZ, a redox active global regulator in Staphylococcus aureus. *J. Biol. Chem. 284*, 23517−23524.
(35) Wu, R. Y., Zhang, R. G., Zagnitko, O., Dementieva, I., Maltzev, N., Watson, J. D., Laskowski, R., Gornicki, P., and Joachimiak, A. (2003) Crystal structure of Enterococcus faecalis SlyA-like transcriptional factor. *J. Biol. Chem. 278*, 20240−20244.
(36) Lunin, V. V., Evdokimova, E., Kudritska, M., Cuff, M. E., Joachimiak, A., Edwards, A. M., Savchenko, A. The crystal structure of transcriptional regulator PA4135, Unpublished work, PDB accession mumber 2FBI.
(37) Hamuro, Y., Burns, L., Canaves, J., Hoffman, R., Taylor, S., and Woods, V. (2002) ) Domain organization of D-AKAP2 revealed by enhanced deuterium exchange-mass spectrometry (DXMS). *J. Mol. Biol. 321*, 703−714.
(38) Wales, T. E., and Engen, J. R. (2006) Hydrogen exchange mass spectrometry for the analysis of protein dynamics. *Mass Spectrom. Rev. 25*, 158−170.
(39) Hong, M., Fuangthong, M., Helmann, J. D., and Brennan, R. G. (2005) Structure of an OhrR-ohrA operator complex reveals the DNA binding mechanism of the MarR family. *Mol. Cell 20*, 131−141.
(40) Brzovic, P. S., Le Trong, I., Navarre, W. W., Fang, F. C., Stenkamp, R. E., Libby, S. J. Crystal structure of transcription regulatory protein slyA from *Salmonella typhimurium* in complex with salicylate ligands. Unpublished work, PDB accession mumber 3DEU.
(41) Hvidt, A., and Nielsen, S. O. (1966) Hydrogen exchange in proteins. *Adv. Protein Chem. 21*, 287−386.
(42) Kaltashov, I. A., and Eyles, S. J. (2002) Studies of biomolecular conformations and conformational dynamics by mass spectrometry. *Mass Spectrom. Rev. 21*, 37−71.
(43) Perera, I. C., Lee, Y. H., Wilkinson, S. P., and Grove, A. (2009) Mechanism for attenuation of DNA binding by MarR family transcriptional regulators by small molecule ligands. *J. Mol. Biol. 390*, 1019−1029.
(44) Aura, A. M., O'Leary, K. A., Williamson, G., Ojala, M., Bailey, M., Puupponen-Pimia, R., Nuutila, A. M., Oksman-Caldentey, K. M., and Poutanen, K. (2002) Quercetin derivatives are deconjugated and converted to hydroxyphenylacetic acids but not methylated by human fecal flora in vitro. *J. Agric. Food Chem. 50*, 1725−1730.
(45) Gross, M., Pfeiffer, M., Martini, M., Campbell, D., Slavin, J., and Potter, J. (1996) The quantitation of metabolites of quercetin flavonols in human urine. *Cancer Epidemiol. Biomarkers Prev. 5*, 711−720.
(46) Tettelin, H., Saunders, N. J., Heidelberg, J., Jeffries, A. C., Nelson, K. E., Eisen, J. A., Ketchum, K. A., Hood, D. W., Peden, J. F., Dodson, R. J., Nelson, W. C., Gwinn, M. L., DeBoy, R., Peterson, J. D., Hickey, E. K., Haft, D. H., Salzberg, S. L., White, O., Fleischmann, R. D., Dougherty, B. A., Mason, T., Ciecko, A., Parksey, D. S., Blair, E., Cittone, H., Clark, E. B., Cotton, M. D., Utterback, T. R., Khouri, H., Qin, H., Vamathevan, J., Gill, J., Scarlato, V., Masignani, V., Pizza, M., Grandi, G., Sun, L., Smith, H. O., Fraser, C. M., Moxon, E. R., Rappuoli, R., and Venter, J. C. (2000) Complete genome sequence of Neisseria meningitidis serogroup B strain MC58. *Science 287*, 1809−1815.
(47) Hanahan, D. (1983) Studies on transformation of Escherichia coli with plasmids. *J. Mol. Biol. 166*, 557−580.
(48) Studier, F. W., and Moffatt, B. A. (1986) Use of bacteriophage T7 RNA polymerase to direct selective high-level expression of cloned genes. *J. Mol. Biol. 189*, 113−130.